

Classical simulation of relativistic quantum mechanics in periodic optical structures

S. Longhi

Received: 16 April 2011 / Published online: 9 July 2011

© Springer-Verlag 2011

Abstract Spatial and/or temporal propagation of light waves in periodic optical structures offers a unique possibility to realize in a purely classical setting the optical analogues of a wide variety of quantum phenomena rooted in relativistic wave equations. In this work a brief overview of a few optical analogues of relativistic quantum phenomena, based either on spatial light transport in engineered photonic lattices or on temporal pulse propagation in Bragg grating structures, is presented. Examples include spatial and temporal photonic analogues of the Zitterbewegung of a relativistic electron, Klein tunneling, vacuum decay and pair production, the Dirac oscillator, the relativistic Kronig–Penney model, and optical realizations of non-Hermitian extensions of relativistic wave equations.

1 Introduction

Quantum–classical analogies have been explored on many occasions to mimic at a macroscopic level many quantum phenomena which are currently inaccessible in microscopic quantum systems [1]. The study of analogies, besides being fruitful in gaining insights into different phenomena in nature, provides a noteworthy strategy in research capable of transferring ideas, concepts, and techniques among apparently unrelated physical fields. In particular, in the past two decades engineered photonic structures have provided a useful laboratory tool to investigate and visualize with classical optics the dynamical aspects embodied in a

wide variety of coherent quantum phenomena encountered in atomic, molecular, condensed-matter, and matter-wave physics [2]. The study of quantum-optical analogies has been greatly stimulated by the development of the field of discrete optics, aimed to realize novel functionalized optical materials based on evanescently coupled optical waveguides in which the dispersion and diffraction properties of light can be specifically managed [3–5]. The development of recent and reliable technologies in waveguide fabrication, notably the one based on waveguide inscription in transparent glasses based on femtosecond laser writing [5], has enabled us to access in the laboratory a wide variety of fascinating optical analogues of quantum systems. Such analogies have also transferred into optics some important ideas and methods for molding the flow of light originally developed in the context of quantum control [2, 6]. Among the wide variety of quantum-optical analogies investigated in the last two decades, we mention the optical analogues of electronic Bloch oscillations [3, 7–12] and Zener tunneling [13–18], dynamic localization [19–27], coherent enhancement and destruction of tunneling [28–30], adiabatic stabilization of atoms in ultra-strong laser fields [31, 32], Anderson localization [33, 34], the quantum Zeno effect [35–37], Rabi flopping [38, 39], coherent population transfer [40–44], coherent vibrational dynamics [45, 46], geometric potentials [47, 48], and dynamical (Kapitza) trapping [49]. Most of such analogies are based on the formal similarity between the paraxial optical wave equation in dielectric media and the single-particle non-relativistic Schrödinger equation, thus providing a test bed for classical analogue studies of non-relativistic quantum phenomena. Optical analogues of many-body phenomena in non-relativistic models, such as photonic analogues of the famous Bose–Hubbard model, have been proposed as well [50–52].

S. Longhi (✉)
Dipartimento di Fisica, Politecnico di Milano, Piazza
L. da Vinci 32, 20133 Milano, Italy
e-mail: stefano.longhi@fisi.polimi.it

Recently, great attention has been devoted toward the investigation of experimentally accessible and controllable classical or quantum systems that simulate certain fundamental phenomena rooted in the relativistic wave equations, such as the Dirac equation for fermionic particles. Among others, cold trapped atoms, ions, and graphene have proven to provide accessible systems to simulate relativistic physics in the laboratory, and a vast literature on this subject has appeared in the past few years (see, for instance, [53–71] and references therein). In particular, low-energy non-relativistic two-dimensional electrons in graphene obey the Dirac–Weyl equation and behave like massless relativistic particles. This has led to the predictions in condensed-matter physics and atom optics of phenomena analogous to Zitterbewegung [72] and Klein tunneling [73] of relativistic massive or massless particles, with the first experimental evidence of Klein tunneling in graphene [74, 75], carbon nanotubes [76], and trapped ions [77] and of Zitterbewegung [78].

Photonic analogues of Dirac-type equations have also been theoretically proposed for light propagation in certain triangular or honeycomb photonic crystals, which mimic the conical singularity of energy bands of graphene [79–86], as well as in metamaterials [87–89], optical superlattices [90–93], Bragg gratings [94–96], and nonlinear quadratic media [97]. Such studies have motivated extended investigations of the properties of ‘photonic graphene’ [79–83, 85, 86, 98–102] and to the proposals of photonic analogues of relativistic phenomena like Zitterbewegung [84, 87–90, 97], Klein tunneling [85–89, 91, 94], decay of the quantum vacuum and pair production [92], the Dirac oscillator [95], and the relativistic versions of the Kronig–Penney model and surface Tamm states [96]. Noticeably, the introduction of gain and/or loss regions in the optical medium can be exploited to realize in a classical setting certain non-Hermitian relativistic models proposed in the context of non-Hermitian quantum mechanics and quantum field theories [103, 104].

In this article a brief overview of a few important optical analogues of relativistic quantum phenomena is presented. Among the various optical realizations of relativistic wave equations proposed in the recent literature and briefly mentioned in the previous discussion, the present work focuses mostly on a few rather simple periodic optical structures, namely spatial light transport in evanescently coupled waveguide arrays and temporal pulse propagation in Bragg grating structures. Specific examples of quantum-optical analogies discussed in the work include spatial and temporal photonic analogues of Zitterbewegung, Klein tunneling, instability of the quantum vacuum and pair production, the Dirac oscillator, the relativistic Kronig–Penney model, and optical simulations of non-Hermitian relativistic wave equations.

2 Photonic Zitterbewegung

Originally predicted by Schrödinger in the study of the Dirac equation [105], Zitterbewegung (ZB) refers to the trembling motion of a freely moving relativistic quantum particle that arises from the interference between the positive (electron) and negative (positron) energy states of the spinor wave function [72, 106]. For a free electron, the Dirac equation predicts the ZB to have an extremely small amplitude (of the order of the Compton wavelength $\simeq 10^{-12}$ m) and an extremely high frequency ($\simeq 10^{21}$ Hz), making such an effect experimentally inaccessible. Moreover, the physical relevance of ZB in relativistic quantum mechanics is a rather controversial issue, because such an effect arises in the framework of the single-particle picture of the Dirac equation, but not in quantum field theory. Phenomena analogous to ZB, which underlie the same mathematical model of the Dirac equation, have so far predicted in a wide variety of quantum and even classical physical systems, as discussed in the introduction. Here we briefly present two optical simulations of the relativistic ZB, based the former on spatial light propagation in binary waveguide arrays, the latter on the frequency conversion process of optical pulses in quadratic nonlinear media.

2.1 Photonic Zitterbewegung in binary waveguide arrays

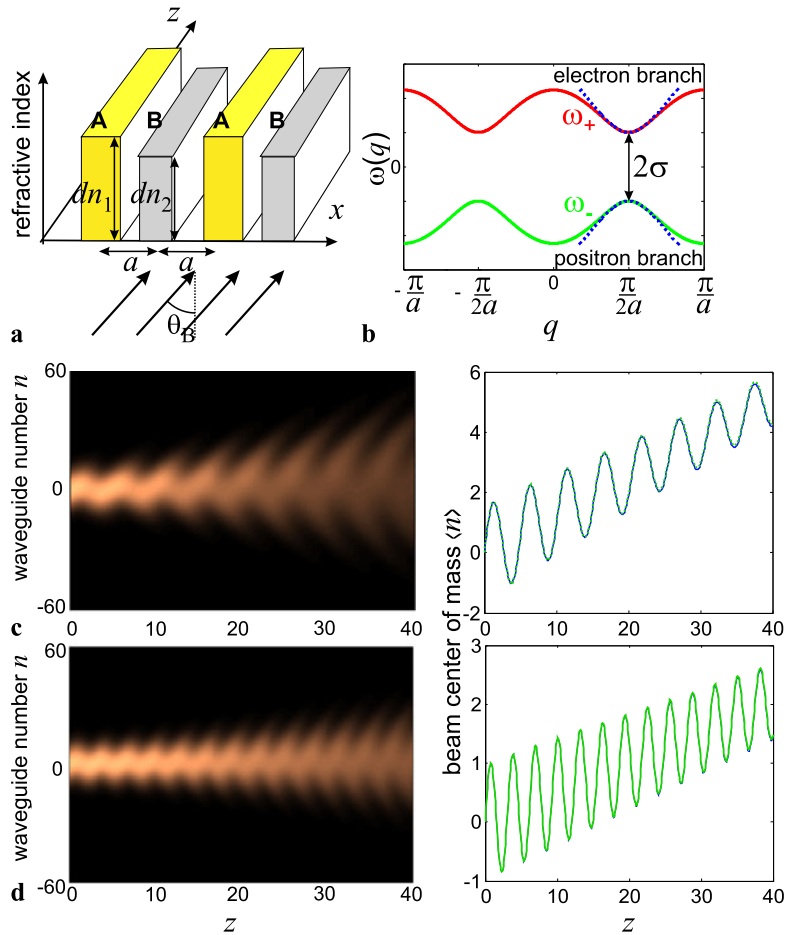
The simplest example in optics where one can find an analogue of the relativistic ZB may be the discrete transport of light waves in a one-dimensional binary array [90]. Such an optical system behaves, in fact, like a one-dimensional superlattice, in which the two minibands of the superlattice play the same role as the positive- and negative-energy branches of the Dirac equation [107]. Under excitation by a broad light beam near the Bragg angle, the discretized light propagates along the array showing a characteristic trembling motion, which mimics the relativistic ZB of the electronic wave function. Such an oscillatory motion has been recently observed in Ref. [93] in binary arrays written in fused silica by femtosecond laser writing technology [5], providing the first simulation in optics of ZB.

Let us consider light propagation in a binary waveguide array, realized by two interleaved lattices A and B, as shown in Fig. 1a. In practice, the superlattice can be realized by a sequence of equally spaced waveguides with alternating deep/shallow peak refractive index changes d_{n1} and d_{n2} . In the tight-binding approximation, light transport is described by the coupled-mode equations [90, 93]

$$i \frac{dc_l}{dz} = -\kappa(c_{l+1} + c_{l-1}) + (-1)^l \sigma c_l, \quad (1)$$

Fig. 1 Photonic analogue of relativistic Zitterbewegung in a binary waveguide array.

- (a) Schematic of the optical superlattice (refractive index change profile $n(x) - n_s$).
- (b) Dispersion curves of the two minibands of the superlattice, corresponding to the electron and positron energy branches of the Dirac equation.
- (c) Evolution of a broad Gaussian beam (snapshot of $|c_n(z)|^2$, left-hand panel), exciting the binary array and tilted at the Bragg angle, and corresponding beam trajectory (right-hand panel), for parameter values $\kappa = 1$ and $\sigma = 0.6$.
- (d) Same as (c), but for $\sigma = 1$



where c_l are the modal field amplitudes in the various waveguides and 2σ and κ are the propagation constant mismatch and the coupling rate between two adjacent waveguides of the array, respectively. The superlattice supports two minibands, separated by a narrow gap of width 2σ (see Fig. 1b), defined by the dispersion curves $\omega_{\pm}(q) = \pm\sqrt{\sigma^2 + 4\kappa^2 \cos^2(qa)}$, where $2a$ is the lattice period and q the Bloch wave number. Hence, in the vicinity of the edges of the first Brillouin zone, e.g. near $q = \pi/(2a)$, the dispersion curves of the two minibands form two opposite hyperbolas, and therefore mimic the typical hyperbolic energy-momentum dispersion relation for positive-energy and negative-energy branches of a freely moving relativistic massive particle (dotted graph). This suggests that light transport in the lattice for Bloch waves with wave number q close to $\pi/(2a)$ simulates the temporal dynamics of the relativistic Dirac equation. When launching a tilted broad beam $E(x, z)$ at the Bragg angle $\theta_B \simeq \lambda/(4n_s a)$ (n_s is the substrate refractive index) into the array, only a small region around $q = \pi/(2a)$ in q -space is excited. After setting $c_{2n}(z) = (-1)^n \psi_1(n, z)$ and $c_{2n-1} = -i(-1)^n \psi_2(n, z)$ and introducing the continuous transverse coordinate $\xi \leftrightarrow n = x/(2a)$, the two-component spinor $\psi(\xi, z) = (\psi_1, \psi_2)^T$ sat-

isfies the one-dimensional Dirac equation [90, 107]

$$i \frac{\partial \psi}{\partial z} = -i\kappa \sigma_x \frac{\partial \psi}{\partial \xi} + \sigma \sigma_z \psi, \quad (2)$$

where $\sigma_x = \begin{pmatrix} 0 & 1 \\ 1 & 0 \end{pmatrix}$ and $\sigma_z = \begin{pmatrix} 1 & 0 \\ 0 & -1 \end{pmatrix}$ are the σ_x and σ_z Pauli matrices. Equation (2) corresponds to the one-dimensional Dirac equation for a relativistic freely moving particle of mass m [106] provided that the formal change

$$\kappa \rightarrow c, \quad \sigma \rightarrow mc^2/\hbar \quad (3)$$

is made, and ξ and z are interpreted as the spatial and the temporal variables, respectively. Therefore, in the optical superlattice the *temporal* evolution of the Dirac spinor wave function ψ is mapped onto the *spatial* evolution along z of the field amplitudes ψ_1 and ψ_2 , describing the occupation amplitudes of light in the two sub-lattices A and B of the binary array. Correspondingly, ZB is observed as a quivering spatial oscillatory motion of the beam center of mass $\langle n \rangle(z) = \sum_n n|c_n|^2 / \sum_n |c_n|^2$. Note that the measurable quantity $\langle n \rangle(z)$ is directly related to the expectation

value of the position for the relativistic particle,

$$\langle \xi \rangle(z) = \left(\int d\xi \xi (|\psi_1|^2 + |\psi_2|^2) \right) / \left(\int d\xi (|\psi_1|^2 + |\psi_2|^2) \right),$$

by the simple relation $\langle n \rangle \simeq 2\langle \xi \rangle + 1/2$ [90]. Let us indicate by $E(x, 0)$ the electric field envelope that excites the superlattice at the $z = 0$ input. For beam incidence close to the Bragg angle θ_B , one can write $E(x, 0) = G(x) \exp(2\pi i x n_s \theta_B / \lambda)$, where the envelope G varies slowly over the waveguide spacing a . Under such an assumption, an exact expression for $\langle \xi \rangle(z)$ can be derived and reads [90]

$$\langle \xi \rangle(z) = \langle \xi \rangle(0) + v_0 z + 2\pi\kappa\sigma^2 \int dk (1/\epsilon^3) \sin(2\epsilon z) |\hat{G}(k)|^2, \quad (4)$$

where $k = 2qa - \pi$ is the shifted transverse momentum, $\epsilon(k) = \sqrt{\sigma^2 + \kappa^2 k^2}$ defines the energy-momentum dispersion relation of the free relativistic particle, $\hat{G}(k) = (1/2\pi) \int d\xi G(2a\xi) \exp(-ik\xi)$ is the angular spectrum of the beam envelope (normalized such that $\int dk |\hat{G}(k)|^2 = 1/4\pi$), and $v_0 = 4\pi\kappa^3 \int dk (k/\epsilon)^2 |\hat{G}(k)|^2$ is the mean particle speed. The last oscillatory term on the right-hand side of (4), superimposed to the straight trajectory defined by the first two terms, is the ZB. For $\hat{G}(k)$ centered at $k = 0$, at leading order (4) yields $\langle \xi \rangle(z) \simeq \langle \xi \rangle(0) + v_0 z + (\kappa/2\sigma) \sin(2\sigma z)$, i.e. the amplitude and frequency of the ZB are given by

$$R_{\text{ZB}} = \kappa/(2\sigma) = \hbar/(2mc), \quad (5)$$

$$\omega_{\text{ZB}} = 2\sigma = 2mc^2/\hbar, \quad (6)$$

respectively. Therefore, ZB vanishes for either the far-relativistic ($m \rightarrow 0$) or the weak-relativistic ($m \rightarrow \infty$) limits: in the first case the amplitude of ZB diverges, but the oscillation frequency ω_{ZB} goes to zero, whereas in the latter case the frequency of ZB diverges but its amplitude vanishes (see, for instance, [107]). As an example, Fig. 1c and d show the ZB as obtained by numerical simulations of the coupled-mode equations for two values of the detuning σ and for a broad Gaussian beam that excites the array at the Bragg angle. The damping of the oscillations observed in the figure is related to the spectral angular broadening of the incident beam [90]. The previous analysis can be extended to a photonic superlattice in two transverse spatial dimensions x and y . The superlattice is composed by two interleaved triangular lattices, with a propagation constant detuning σ between the guided modes, and a broad input beam is launched at the Bragg angle. In this case, in the continuous limit the evolution of the beam envelope along the longitudinal direction z is described by a two-dimensional Dirac-type equation, which reduces to the massless case of the previously studied photonic graphene [79–86] in the limit $\sigma \rightarrow 0$.

2.2 Photonic Zitterbewegung in nonlinear frequency conversion

A second example of a photonic analogue of ZB is provided by the frequency-conversion process of optical pulses in a nonlinear quadratic medium arising from group-velocity mismatch [97]. Let us consider the propagation of three optical pulses at carrier frequencies ω_1 , ω_2 , and $\omega_3 = \omega_1 + \omega_2$ in a nonlinear quadratic medium and in the presence of group-velocity mismatch. To study the analogue of ZB in the frequency-conversion process, we assume that at the input plane $z = 0$ the nonlinear crystal is excited by a strong and nearly continuous-wave pump field at frequency ω_1 , and by a weak and short signal pulse at frequency ω_2 and temporal profile $g(t)$. Assuming that group-velocity dispersion is negligible and assuming perfect phase matching, in the no-pump-depletion approximation the sum-frequency generation process is described by the two coupled wave equations

$$\left(\frac{\partial}{\partial z} + \frac{1}{v_{g2}} \frac{\partial}{\partial t} \right) A_2 = -i\kappa A_3, \quad (7)$$

$$\left(\frac{\partial}{\partial z} + \frac{1}{v_{g3}} \frac{\partial}{\partial t} \right) A_3 = -i\kappa A_2, \quad (8)$$

where A_l ($l = 2, 3$) is the amplitude of the electric field envelope at frequency ω_l , normalized such that $|A_l|^2$ ($l = 2, 3$) is the photon flux at frequency ω_l , v_{gl} is the group velocity in the medium at frequency ω_l , $\kappa = \rho \sqrt{I_1/\hbar\omega_1}$, ρ is the strength of the nonlinear interaction, and I_1 is the intensity of the pump field. The coupled equations (7) and (8) can be cast in a Dirac form after introduction of the coordinates of a moving frame

$$\xi = z, \quad \eta = t - z/v_g, \quad (9)$$

where the velocity v_g is defined by the relation

$$\frac{1}{v_g} = \frac{1}{2} \left(\frac{1}{v_{g2}} + \frac{1}{v_{g3}} \right). \quad (10)$$

In the moving frame, after introduction of the spinor wave field $\psi = (A_2, A_3)^T$, (7) and (8) can be cast in the form of a Dirac equation

$$i \frac{\partial \psi}{\partial \xi} = -i\sigma_z \delta \frac{\partial \psi}{\partial \eta} + \kappa \sigma_x \psi, \quad (11)$$

where σ_x and σ_z are the Pauli matrices and where we have set

$$\delta = \frac{1}{2} \left(\frac{1}{v_{g2}} - \frac{1}{v_{g3}} \right). \quad (12)$$

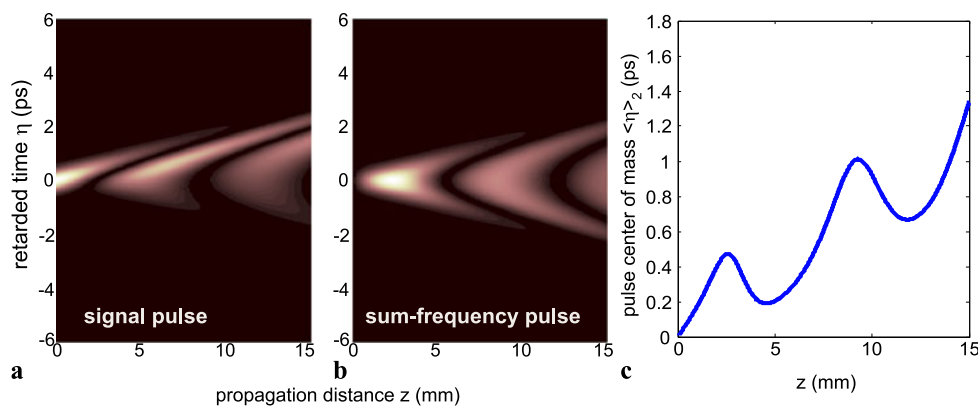


Fig. 2 Zitterbewegung in the process of sum-frequency generation induced by group-velocity mismatch. (a) and (b) show the evolution of the signal and sum-frequency pulse intensities in a 15-mm-long PPLN crystal for a continuous-wave pump. The crystal is excited by a Gaussian signal pulse of duration $\tau_p = 0.5$ ps. In (c) the evolution of the pulse center of mass $\langle \eta \rangle_1$ for the signal wave is depicted. The oscillatory behavior of $\langle \eta \rangle_1$, arising from the group-velocity mismatch between signal and sum-frequency fields, is a signature of ZB

sian signal pulse of duration $\tau_p = 0.5$ ps. In (c) the evolution of the pulse center of mass $\langle \eta \rangle_1$ for the signal wave is depicted. The oscillatory behavior of $\langle \eta \rangle_1$, arising from the group-velocity mismatch between signal and sum-frequency fields, is a signature of ZB

Note that, after the formal change

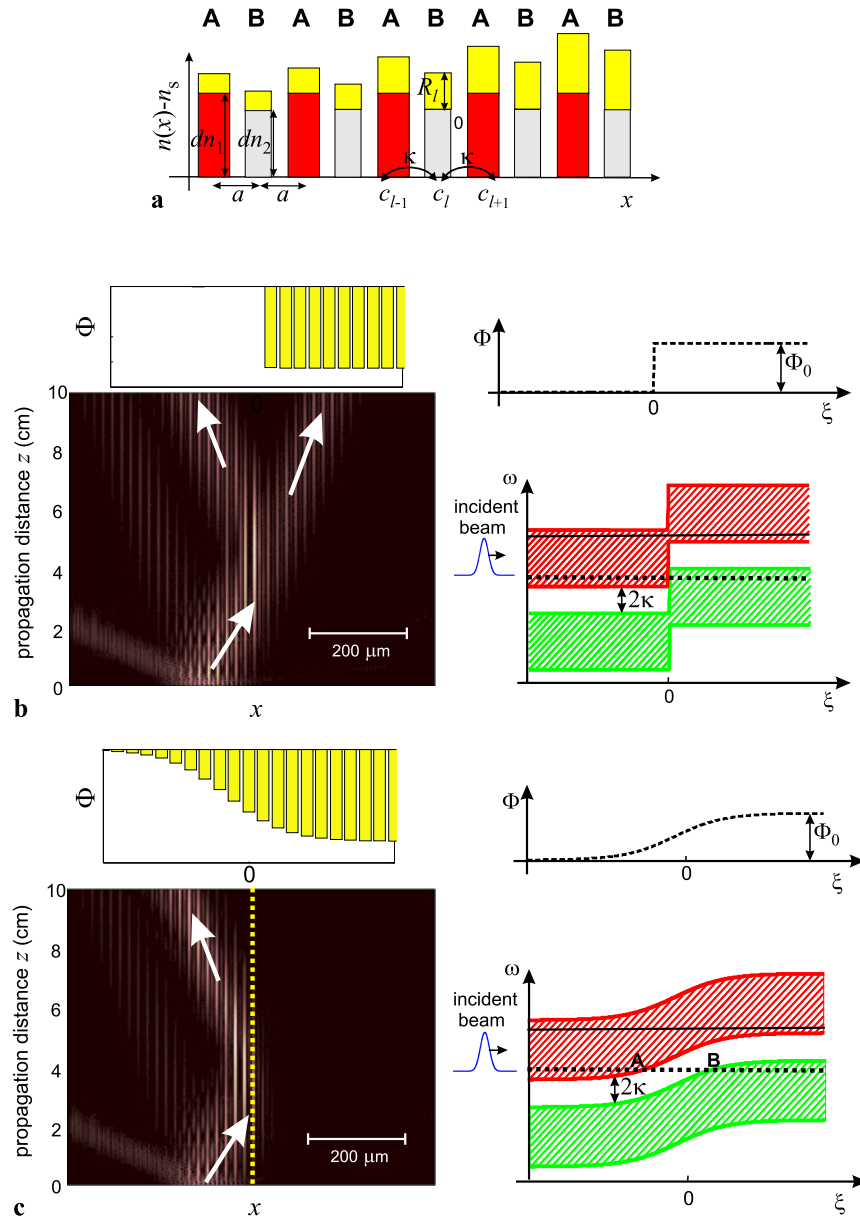
$$\begin{aligned} \delta &\rightarrow c, \\ \kappa &\rightarrow \frac{mc^2}{\hbar}, \\ \xi &\rightarrow t, \quad \eta \rightarrow x. \end{aligned} \quad (13)$$

Equation (11) corresponds to the one-dimensional Dirac equation for a relativistic particle of mass m in the absence of external fields, moving along the x axis, written in the Weyl representation [106]. Such a representation is different, though equivalent, to the one used in the previous subsection (compare (11) with (2)), the spinor components in the two representations being related by a unitary transformation. Therefore, the *temporal* evolution of the spinor wave function ψ for the Dirac particle is mapped into the *spatial* evolution of the envelopes A_2 and A_3 for signal and sum-frequency pulses, respectively, whereas the spatial coordinate of the Dirac particle is mapped into the retarded time η of the optical pulses. In the absence of group-velocity mismatch, the massless Dirac equation is obtained, in which ZB vanishes. As an example, Fig. 2 shows ZB in the process of sum-frequency generation which applies to a periodically poled lithium niobate (PPLN) crystal with a quasi-phase-matched grating that ensures phase matching at the wavelengths $\lambda_1 = 1550$ nm (pump), $\lambda_2 = 810$ nm (signal), and $\lambda_3 = 532$ nm (sum-frequency). The crystal is pumped by a near-continuous-wave pump of intensity $I = 1$ MW/cm² and excited at the input plane by a short Gaussian signal pulse of duration $\tau_p = 0.5$ ps. The mismatch of the group velocities of signal and sum-frequency fields clearly results in an oscillating motion (jitter) of the signal pulse along the propagation in the nonlinear crystal, which is the signature of ZB.

3 Photonic analogues of Klein tunneling

A remarkable prediction of the Dirac equation is that a below-barrier electron can pass a large repulsive and *sharp* potential step without the exponential damping expected for a non-relativistic particle. Such a transparency effect, originally predicted by Klein [73] and referred to as Klein tunneling (KT), arises from the existence of negative-energy solutions of the Dirac equation and requires a potential step height ΔV of the order of twice the rest energy mc^2 of the electron [108]. Relativistic tunneling across a *smooth* potential step, which describes the more physical situation of a constant electric field E in a finite region of space of length l , was subsequently studied by Sauter [109]. Sauter showed that to observe barrier transparency the potential increase $\Delta V \simeq eEl$ should occur over a distance l of the order of or smaller than the Compton wavelength $\lambda_C = \hbar/(mc)$, the transmission probability rapidly decaying toward zero for a smoother potential increase [108–110]. The required field corresponds to the critical field for e^+e^- pair production in vacuum, and its value is extremely strong making the observation of relativistic KT for electrons very challenging. Therefore, growing efforts have been devoted to finding experimentally accessible systems to investigate analogues of relativistic KT, as discussed in the introduction. In particular, based on the interesting property that electrons in graphene near a Dirac point of the band structure behave like massless Dirac particles, solid-states analogues of KT have been proposed and experimentally demonstrated quite recently. In optics, several proposals of KT analogues have been suggested as well in the past few years, as discussed in the introduction. An important optical setup is provided by light transport in honeycomb photonic lattices, the so-called photonic graphene, whose band structure mimics the one of graphene [85, 86]. However, even in simpler one-

Fig. 3 Photonic analogue of relativistic Klein tunneling in a binary waveguide array with an interface. (a) Schematic of the optical superlattice. (b) Beam refraction across a potential step, corresponding to KT. (c) Absence of beam refraction, corresponding to inhibition of KT, for a smooth potential barrier. The right-hand panels in (b) and (c) depict the space-energy band diagram, clearly explaining the inhibition of tunneling in (c)



dimensional periodic optical structures one can realize optical analogues of KT [91, 94]. Here we briefly discuss two of such simple realizations. The former one is based on monochromatic light propagation in waveguide superlattices [91], whereas the latter one is based on temporal pulse propagation in fiber Bragg gratings [94].

3.1 Photonic Klein tunneling in optical superlattices

As in Sect. 2.1, let us consider the transport of monochromatic discretized light waves in a binary array of waveguides, realized by two interleaved lattices A and B. As compared to the superlattice used to realize ZB (Fig. 1a), here a weak modulation R_l of the index change, much smaller than

either dn_1 or dn_2 and equal for the interleaved lattices A and B, i.e. such that $R_{2l-1} = R_{2l}$, is superimposed to the lattice, as shown in Fig. 3a. Light transport in the superlattice is then described by the coupled-mode equations (compare with (1))

$$i \frac{dc_l}{dz} = -\kappa(c_{l+1} + c_{l-1}) + (-1)^l \sigma c_l + \Phi_l c_l, \quad (14)$$

where the weak modulation R_l of the refractive-index change is responsible, at leading order, to a slight change Φ_l of the modal propagation constants in the various waveguides. For a broad beam exciting the superlattice tilted close to the Bragg angle, in the continuous limit light transport turns out to be described by the Dirac wave equation (com-

pare with (2))

$$i\frac{\partial\psi}{\partial z} = -ik\sigma_x\frac{\partial\psi}{\partial\xi} + \sigma\sigma_z\psi + \Phi(\xi)\psi, \quad (15)$$

where $\Phi(\xi) = \Phi_{2l} = \Phi_{2l-1}$. Note that (15) is formally analogous to the one-dimensional Dirac equation for an electron of mass m in the presence of an electrostatic potential $\Phi(x)$, once the formal substitutions (3) are made (see, for instance, [106]). Therefore, by engineering the refractive-index depths of the various waveguides in the array, a step-like potential $\Phi(\xi)$ at $\xi = 0$ can be realized. KT can be observed as a beam transmission (refraction) across the interface [91]. By varying the steepness of the potential step, the optical superlattice can be designed to demonstrate the disappearance of KT in a smooth potential step as well, i.e. the transition from KT for a steep potential to Sauter's tunneling suppression for a smooth potential step. In the optical context, Sauter's inhibition of light tunneling at a smooth interface can be explained by considering the space-dependent band structures of the tight-binding superlattices, as shown in Fig. 3. Such bands are similar to the energy band diagrams of a semiconductor, in which the two superlattice minibands (i.e. the electron and positron energy branches of the Dirac equation) play the role of the conduction and valence bands and the effect of the external potential $\Phi(\xi)$ is to curve the band structure. For a sharp potential step (Fig. 3b) at the interface $\xi = 0$, the electron and positron energy bands are overlapped, and the beam does not need to cross any forbidden region, i.e. KT occurs. However, owing to the sharp discontinuity of media properties, beam transmission is not complete, and some light is reflected as in a Fresnel discontinuity between two different dielectric media. Conversely, for a smooth potential step (see Fig. 3c) the beam has to cross a forbidden region, which behaves like a potential barrier. The width of the potential barrier is indicated by the segment AB in Fig. 3c. Because the width AB increases as the potential step becomes smoother, the corresponding tunneling probability, i.e. beam transmission across the interface, rapidly decreases. This explains the inhibition of KT and the transition to Sauter's regime [109].

3.2 Photonic Klein tunneling in fiber Bragg gratings

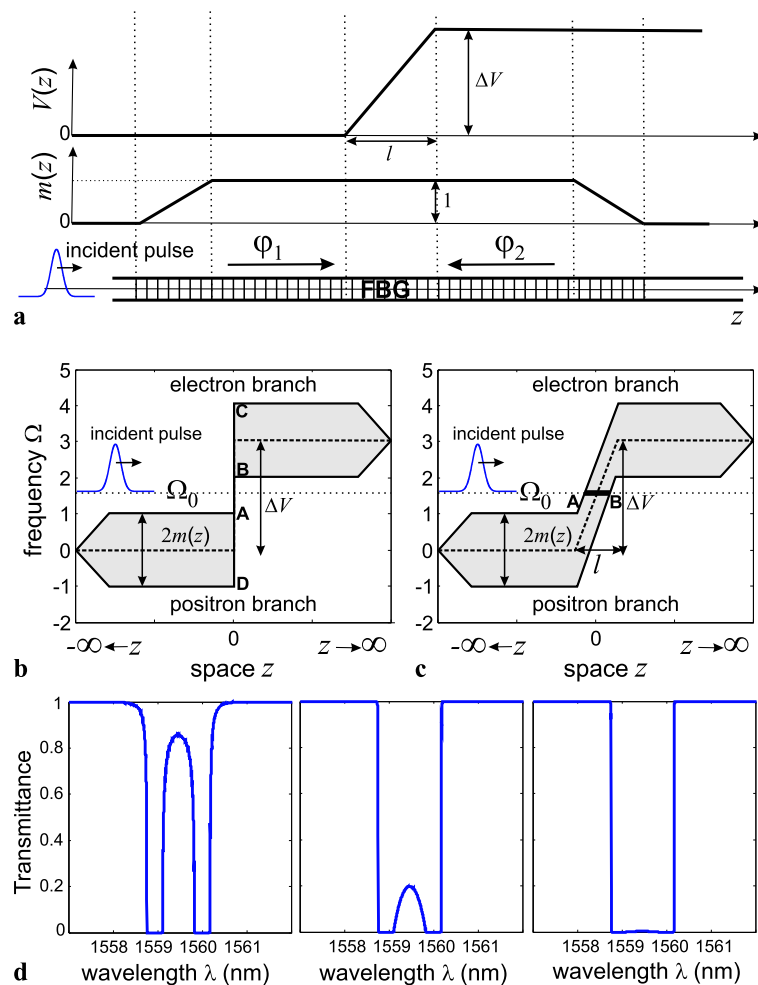
Another rather simple optical realization of Klein tunneling is provided by photonic tunneling in structured fiber Bragg gratings (FBGs) [94]. In a FBG, the effective index of the fiber is modulated along the longitudinal z' direction according to $n(z') = n_0 + \Delta n m(z') \cos[2\pi z'/\Lambda + 2\phi(z')]$, where n_0 is the effective mode index in the absence of the grating, $\Delta n \ll n_0$ is the peak index change of the grating, Λ is the nominal period of the grating defining the reference frequency $\omega_B = \pi c / (\Lambda n_0)$ of Bragg scattering, c is

the speed of light in vacuum, and $m(z')$ and $2\phi(z')$ describe the slow variation, as compared to the scale of Λ , of normalized amplitude and phase, respectively, of the index modulation. Note that the local spatial frequency of the grating is $k(z') = 2\pi/\Lambda + 2(d\phi/dz')$, so that the local chirp rate is $C = dk/dz' = 2(d^2\phi/dz'^2)$. The periodic index modulation leads to Bragg scattering between two counterpropagating waves at frequencies close to ω_B . By letting $E(z', t) = \varphi_1(z', t) \exp[-i\omega_B t + ik_B z' + i\phi(z')] + \varphi_2(z', t) \exp[-i\omega_B t - ik_B z' - i\phi(z')] + c.c.$ for the electric field in the fiber, where $k_B = \pi/\Lambda$, the envelopes φ_1 and φ_2 of counterpropagating waves satisfy coupled-mode equations. After introduction of the dimensionless variables $z = z'/Z$ and $\tau = t/T$, with characteristic spatial and time scales $Z = 2n_0/(k_B \Delta n)$ and $T = Z/v_g$, and the new envelopes $\psi_{1,2}(z') = [\varphi_1(z') \mp \varphi_2(z')]/\sqrt{2}$, the coupled-mode equations can be cast in the Dirac form [94]

$$i\partial_\tau\psi = -i\sigma_x\partial_z\psi + m(z)\sigma_z\psi + V(z)\psi \quad (16)$$

for the spinor wave function $\psi = (\psi_1, \psi_2)^T$, where $V(z) = (d\phi/dz)$, v_g is the group velocity at the Bragg frequency, and $\sigma_{x,z}$ are the Pauli matrices. In its present form, (16) is formally analogous to the one-dimensional Dirac equation with $\hbar = c = 1$ in the presence of an external electrostatic potential $V(z)$, m playing the role of a dimensionless (and generally space-dependent) rest mass (see, for instance, [108, 110]). The optical analogue of the forbidden energy region of the Dirac equation, in this case, simply corresponds to the photonic stop band of the periodic grating. As the refractive-index modulation of the grating, i.e. the mass term m in the Dirac equation (16), is decreased, the stop-band region shrinks and the limit of a massless Dirac equation (similar to the one describing the dynamics of electrons in graphene near a Dirac point) is attained. The additional external potential V in (16), related to the phase modulation of the grating according to $V(z) = d\phi/dz$, changes the local position of the forbidden energy region. Therefore, pulse propagation in a FBG with suitably designed phase and amplitude grating profiles can be used to mimic the relativistic tunneling of a wave packet in a potential step $V(z)$. A typical diagram of a structured FBG suited to realize KT and the inhibition of KT for a smooth potential step, together with the space-energy diagram of the grating [94], is shown in Fig. 4a–c. The signatures of KT and of its inhibition for a smooth potential step are simply revealed by spectrally resolved transmission measurements of the grating. In fact, for a sharp potential step a transmission window is opened inside the band gap of the periodic grating, whereas for a smooth potential step tunneling is prevented (according to the diagram of Fig. 4c) and the transmission window inside the gap vanishes. This is shown in Fig. 4d, which depicts typical transmission spectra in three FBGs with different chirp rates, realized to operate near

Fig. 4 Photonic realization of relativistic Klein tunneling in a structured FBG. (a) Schematic of the local period detuning $V = (d\phi/dz)$ (upper plot) and amplitude m (lower plot) profiles of a FBG to observe the optical analogue of KT. (b) and (c) Space-energy band diagrams of the FBG for a sharp (b) and a smooth (c) potential step $V(z)$ of height ΔV . The shaded regions are the forbidden (stop-band) energies, the dotted horizontal line is the frequency Ω_0 of the incoming wave packet, and the dashed curve is the shape of the potential step $V(z)$. (d) Numerically computed spectral transmittance of three FBGs for increasing length of the chirped region (from left to right). The transmission window inside the stop band of the grating for a sharp potential step (left-hand panel) is the signature of KT



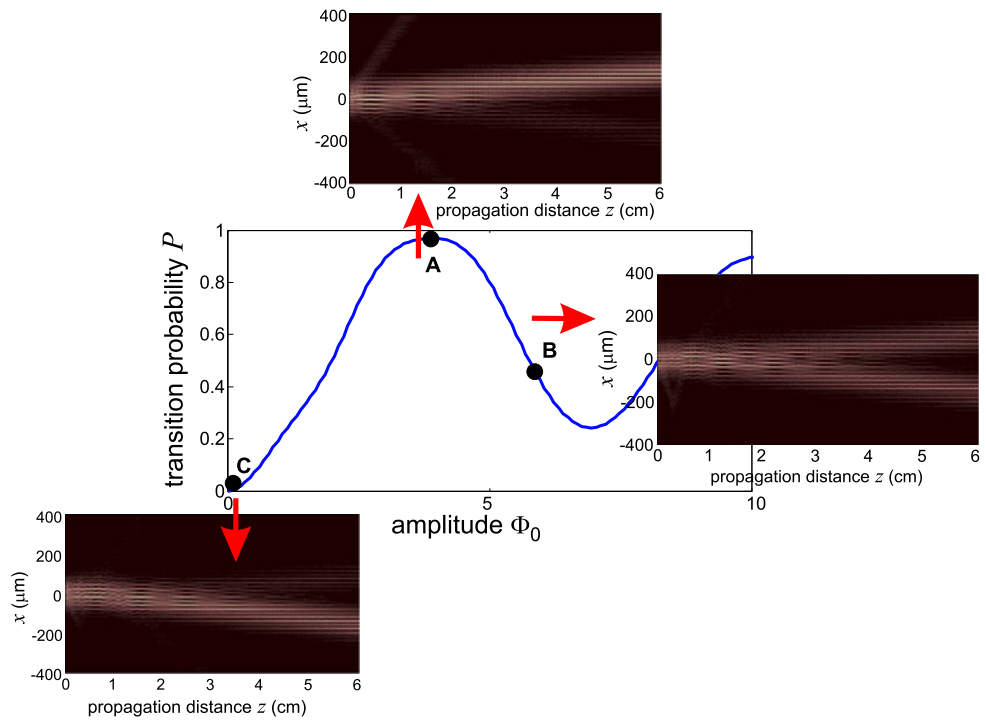
the $\lambda = 1.5 \mu\text{m}$ wavelength of optical communications (for more details see [94]).

4 Optical simulation of vacuum decay and pair production

Electron–positron pair production due to the instability of the quantum electrodynamics (QED) vacuum in an external electric field is another remarkable prediction of Dirac theory and regarded as one of the most intriguing nonlinear phenomena in QED, whose experimental observation is still lacking (see, for instance, [111, 112]). In intuitive terms and in the framework of one-particle Dirac theory, the pair-production process can be simply viewed as the transition of an electron of the Dirac sea occupying a negative-energy state into a final positive-energy state, leaving a vacancy (positron) in the negative-energy state. There are basically two distinct transition mechanisms: the Schwinger mechanism, induced by an ultra-strong static electric field, and dynamic pair creation, induced by time-varying electric

fields. The Schwinger mechanism [113] is basically a tunneling process through a classically forbidden region, bearing a close connection to Klein tunneling discussed in the previous section. The other mechanism, namely dynamic pair creation, was originally proposed by Brezin and Itzykson [114] for oscillating spatially homogeneous fields, and has recently attracted great attention because of its potential implementation using counterpropagating ultra-strong laser fields. Dynamic pair production is closely related to such intriguing phenomena like Rabi oscillations of the Dirac sea (see, for instance, [112]). In the framework of the one-particle Dirac theory of vacuum decay, a simple picture of pair production is represented by the time evolution of an initially negative-energy Gaussian wave packet, representing an electron in the Dirac sea, under the influence of an oscillating electric field [115]. When the e^+e^- pair is produced, a droplet is separated from the wave packet and moves opposite to the initial one [115]. The droplet is a positive-energy state and represents the created electron. In a recent work [92], it was shown that light transport in a binary waveguide array with a sinusoidally curved optical axis provides a classical simulator of the dynamic pair pro-

Fig. 5 Photonic realization of dynamic e^+e^- pair production in a binary waveguide array with bent optical axis. The figure shows the probability of pair production after the application of a single-cycle ultra-strong laser pulse for increasing values of the amplitude Φ_0 . The insets show the detailed beam evolution along the array corresponding to the amplitudes of A, B, and C. The fractional beams deflected at opposite angles correspond to states in the negative (positron) and positive (electron) energy branches of the Dirac equation



duction process, in which pair production is visualized as a breakup of an initial Gaussian wave packet, composed by a superposition of Bloch modes of the lowest lattice miniband and representing an electron in the Dirac sea. Periodic axis bending of the waveguides mimics the effect of an external ac field, which induces transitions into the upper lattice miniband (the electron energy branch). The optical structure proposed to simulate dynamic pair production is basically the binary superlattice of Fig. 1a; however, the optical axis of the waveguides is now periodically bent along the propagation direction z . If the array is excited by a broad beam tilted close to the Bragg angle, the continuous limit of the coupled-mode equations now leads to the following Dirac equation for the spinor ψ [92] (compare with (2)):

$$i\frac{\partial\psi}{\partial z} = -i\kappa\sigma_x\frac{\partial\psi}{\partial\xi} + \sigma\sigma_z\psi - 2\kappa\Phi(z)\sigma_x\psi, \quad (17)$$

where $\Phi(z)$ accounts for the waveguide axis bending and reads explicitly [92]

$$\Phi(z) = \frac{2\pi n_s a (dx_0/dz)}{\lambda}. \quad (18)$$

In the previous equation, a is the distance between two adjacent waveguides, n_s is the bulk refractive index, λ is the wavelength of light, and $x_0(z)$ is the axis bending profile. Note that, after the formal change

$$\kappa \rightarrow c,$$

$$\sigma \rightarrow \frac{mc^2}{\hbar},$$

$$\xi \rightarrow x, \quad (19)$$

$$\Phi \rightarrow \frac{eA_x}{2\hbar c},$$

$$z \rightarrow t.$$

Equation (17) corresponds to the one-dimensional Dirac equation for an electron of mass m and charge e in the presence of a spatially homogeneous and time-varying vectorial potential $\mathbf{A} = (A_x, 0, 0)$, which describes the interaction of the electron with an external oscillating electric field $E_x(t) = -(\partial A_x / \partial t)$ in the dipole approximation (see, for instance, [106]). Because of momentum conservation, in the spatially homogeneous and time-dependent field the problem of pair creation can be reduced to the transition between two states consisting of a negative- and a positive-energy state coupled by the external field. Within the two-level model, pair production generally occurs as a multi-photon resonance process enforced by energy conservation, with interesting effects such as Rabi oscillations of the quantum vacuum. Pair production induced by an ultra-strong and ultra-short laser pulse can be mimicked by assuming, for instance, a single cycle of the ac field ($\Phi(z) = \Phi_0 \sin(2\pi z/\Lambda)$ for $0 < z < \Lambda$, $\Phi(z) = 0$ for $z < 0$ and $z > \Lambda$). As an example, Fig. 5 shows the behavior of the transition probability P , after the interaction with a single-cycle pulse, as obtained by numerical simulations of the Dirac equation for $\kappa = 2$, $\sigma = 1.817$, $\Lambda = 0.6676$, momentum $q = \pi/(4a)$, and for increasing values of the field amplitude Φ_0 . The detailed beam evolution of an initial Gaussian wave packet along

a waveguide array with single-cycle modulated axis, corresponding to the three conditions A, B, and C of Fig. 5, are depicted in the insets of the figure. The input wave packet is mostly composed by Bloch modes belonging to the lowest miniband of the array, i.e. it belongs to the Dirac sea (the negative-energy branch of the Dirac equation). Owing to the modulation, excitation of the upper miniband, corresponding to the creation of a e^+e^- pair, is clearly observed. Note that, as the wave packets belonging to the two minibands refract at different angles, they separate from each other after some propagation distance. Such a splitting is precisely the signature of e^+e^- pair production, as discussed in [115].

5 Optical simulation of the Dirac oscillator

The relativistic extension of the quantum harmonic oscillator, the so-called Dirac oscillator (DO) [116–118], provides a paradigmatic and exactly solvable model in relativistic quantum mechanics. Originally proposed in quantum chromodynamics in connection to quark confinement models in mesons and baryons [119], the DO has received great interest in relativistic many-body theories and supersymmetric relativistic quantum mechanics (see [117, 118, 120–122] and references therein). The DO model is obtained from the free Dirac equation by the introduction of the external potential via a non-minimal coupling [116, 118, 122]. Since the resulting equation is linear in both momentum and position operators, in the non-relativistic limit a Schrödinger equation with a quadratic potential is then obtained. In spite of the great amount of theoretical studies, the DO model in relativistic quantum mechanics and particle physics remains far from any experimental consideration. In a recent work [95], a photonic realization of the DO, based on light propagation in structured FBGs, has been proposed. The main idea is that, as shown in Sect. 3.2, coupled-mode equations describing forward and backward light coupling in a Bragg grating structure have the form of a Dirac equation. Using the same notation as in Ref. [95] and with reference to Fig. 6a, let us consider light propagation in a FBG with an index grating $n(z) = n_0 + \Delta n h(z) \cos[2\pi z/\Lambda + \phi(z)]$, where n_0 is the effective mode index in the absence of the grating, $\Delta n \ll n_0$ is a reference value of the index change of the grating, Λ is the nominal grating period defining the Bragg frequency $\omega_B = \pi c/(\Lambda n_0)$, c is the speed of light in vacuum, and $h(z)$ and $\phi(z)$ describe the amplitude and phase profiles, respectively, of the grating. To study Bragg scattering of counterpropagating waves at frequencies close to ω_B , let $E(z, t) = \{u(z, t) \exp(-i\omega_B t + 2\pi izn_0/\lambda_0) + v(z, t) \exp(-i\omega_B t - 2\pi izn_0/\lambda_0) + c.c.\}$ be the electric field in the fiber, where $\lambda_0 = 2n_0\Lambda$ is the Bragg wavelength, and the envelopes u and v of counterpropagating waves satisfy coupled-mode equations. After introduction of the dimensionless variables $x = z/Z$ and $\tau = t/T$, with characteristic

spatial and time scales $Z = \lambda_0/(\pi \Delta n)$ and $T = Z/v_g$ (v_g is the group velocity at the Bragg frequency), and the new envelopes $\psi_{1,2}(z) = [u(z) \mp v(z)]/\sqrt{2}$, the coupled-mode equations can be cast in the Dirac form [95]

$$i\partial_\tau \psi = \sigma_x \{p_x - i f(x) \sigma_z\} \psi + \sigma_z m(x) \psi \quad (20)$$

for the spinor wave function $\psi = (\psi_1, \psi_2)^T$, where σ_x and σ_z are the Pauli matrices, $p_x = -i(d/dx)$, and

$$m(x) = h(x) \cos[\phi(x)], \quad f(x) = -h(x) \sin[\phi(x)]. \quad (21)$$

In its present form, (20) is analogous to the one-dimensional Dirac equation [106], written in atomic units ($\hbar = c = 1$), with a space-dependent mass m and with the momentum operator p_x substituted with $p_x - i f(x) \sigma_z$. The space dependence of the particle mass m is known to describe the particle interaction with a scalar Lorentz potential, whereas the substitution $p_x \rightarrow p_x - i f(x) \sigma_z$ corresponds to a non-minimal coupling which is essential to describe the relativistic DO (see, for instance, [122]). To realize the one-dimensional analogue of the DO, let us choose the amplitude h and phase ϕ profiles of the grating such that $h \cos \phi = m_0$ and $h \sin \phi = -f(x) = \omega_s m_0 x$, i.e. (see Fig. 6b)

$$h(x) = m_0 \sqrt{1 + (\omega_s x)^2}, \quad \phi(x) = \text{atan}(\omega_s x), \quad (22)$$

where m_0 and ω_s are two arbitrary constants, corresponding to the particle rest mass and oscillation frequency of the DO in the non-relativistic limit [122]. Analytical expressions of the energy spectrum for the one-dimensional DO and of corresponding bound states can be derived following a standard procedure detailed e.g. in Ref. [122]. Assuming for the sake of definiteness that $\omega_s > 0$, the positive-energy spectrum (electron branch) of the DO is given by

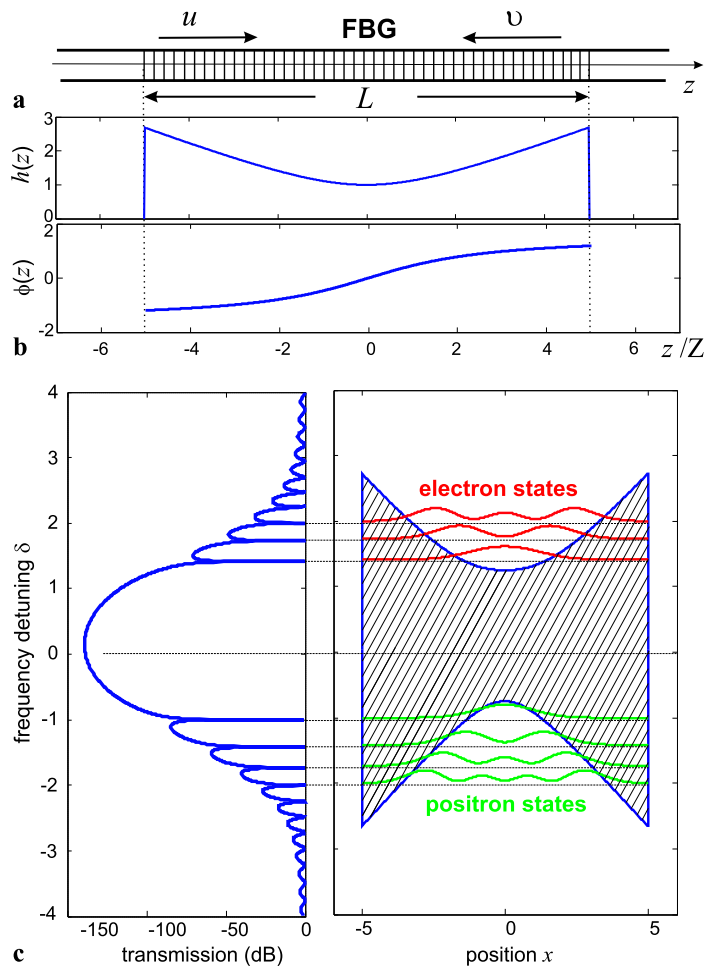
$$\delta_n = \sqrt{m_0^2 + 2m_0\omega_s(1+n)}, \quad n = 0, 1, 2, 3, \dots, \quad (23)$$

whereas the negative-energy spectrum (positron branch) is given by

$$\delta_n = -\sqrt{m_0^2 + 2m_0\omega_s n}, \quad n = 0, 1, 2, 3, \dots. \quad (24)$$

The corresponding eigenfunctions $\psi_\pm(x)$ can be simply expressed in terms of Hermite polynomials multiplied by a Gaussian function. Note that the negative (positron) energy spectrum of the DO is not obtained from the positive (electron) energy spectrum by sign reversal ($\delta \rightarrow -\delta$), the positron branch possessing an additional bound state with energy $\delta = -m_0$. In our FBG realization of the DO, bound states with positive and negative energies should correspond to trapped light states in the FBG with resonance frequencies above ($\delta > 0$) and below ($\delta < 0$) the Bragg frequency ω_B , respectively. In a FBG of finite length, the ideal amplitude profile $h(x)$, defined by (22), must be truncated, i.e. one has

Fig. 6 Photonic realization of the Dirac oscillator in a fiber Bragg grating. (a) Schematic of a FBG. (b) Example of FBG amplitude and phase profiles that realize the analogue of the Dirac oscillator ($m_0 = 1$, $\omega_s = 0.5$, $L/Z = 10$). (c) Numerically computed power transmission (dB units) of a lossless FBG with amplitude and phase profiles shown in (b) (left-hand panel), and corresponding reflection band diagram (dashed area, right-hand panel) with a few low-order intensity profiles of trapped modes in the electron and positron branches



$h(x) = 0$ for $|x| > L/(2Z)$, where L is the grating length (see Fig. 6b). The effect of grating truncation is twofold. First, the bound states of the DO become resonance modes with a finite lifetime, which should thus be observable as narrow transmission peaks embedded in the stop band of the grating. Second, the number of resonance modes sustained by the grating is finite owing to grating truncation. As an example, Fig. 6c shows a typical transmission spectrum (power transmission versus normalized frequency detuning $\delta = (\omega - \omega_B)T$) for a FBG with length $L/Z = 10$ for parameter values $m_0 = 1$ and $\omega_s = 0.5$. In the figure, the corresponding reflection band diagram (dashed area) of the grating in the (x, δ) plane, together with the electron ($\delta > 0$) and positron ($\delta < 0$) levels and a few eigenstates of the DO, are also depicted. The transmission peaks visible in the spectrum of Fig. 6c, embedded in the stop band of the FBG, occur precisely at the values δ_n predicted by (23) and (24). Note the asymmetry of the transmission spectrum around $\delta = 0$, with an additional resonance in the positron ($\delta < 0$) branch of the spectrum with no counterpart in the electron ($\delta > 0$) branch. In an experiment, the resonant states of the DO and the asymmetry of the spectrum can be simply de-

tected from spectrally resolved transmission measurements of the grating using standard techniques.

6 Photonic realization of the relativistic Kronig–Penney model and relativistic surface Tamm states

The Kronig–Penney model for the non-relativistic Schrödinger equation [123] is one among the simplest models in solid-state physics that describes the electronic band structure of an idealized one-dimensional crystal. Relativistic extensions of the Kronig–Penney model (also referred to as the Dirac–Kronig–Penney model) have been discussed by several authors (see, for instance, [124–135] and references therein), and the impact of relativity on the band structure and localization, such as shrinkage of the bulk bands with increasing band number, have been highlighted on many occasions. In earlier studies, the Dirac–Kronig–Penney model also attracted some attention and caused a lively debate about the existence of so-called Dirac surface states, i.e. relativistic surface Tamm states which disappear in the non-relativistic limit [125, 129, 136–141]. In

Ref. [96], a photonic realization of the relativistic Kronig–Penney model and relativistic surface Tamm states has been proposed, which is based on light propagation in superstructure FBGs with phase defects. Light propagation in a FBG with a periodic sequence of phase slips was shown to simulate the relativistic Kronig–Penney model, the band structure of which being mapped into the spectral transmission of the FBG. Similarly, a semi-infinite FBG with phase defects interfaced with a uniform FBG with a different modulation period was shown to support Tamm surface states analogous to the relativistic Tamm states. Such surface states are responsible for narrow resonance peaks in the transmission spectrum of the grating.

Using the same notation as in Sect. 3.2, light propagation in a superstructure FBG is described by the Dirac equation (16), where the scalar (m) and vectorial (V) potential terms entering in the equation are defined by the apodization and phase profiles of the grating, respectively. The Dirac–Kronig–Penney model for an infinitely extended lattice corresponds to a constant mass $m(z) = m_0$ and to a potential $V(z)$ given by the superposition of equally spaced δ -like barriers, namely [124]

$$V(z) = V_0 \sum_{n=-\infty}^{\infty} \delta(z - na), \quad (25)$$

where $V_0 > 0$ is the area of the barrier and a is the lattice period. Stationary solutions $\psi(z, \tau) = \psi_0(z) \exp(-iE\tau)$ to the Dirac equation (16) in the periodic potential (25) with energy E are of Bloch–Floquet type, i.e. $\psi_0(z + a) = \psi_0(z) \exp(iqa)$, where q is the Bloch wave number which varies in the first Brillouin zone ($-\pi/a \leq q < \pi/a$). The corresponding energy spectrum is composed by a set of allowed energy bands $E = E(q)$, which are defined by the following implicit equation (see, for instance, [139]):

$$\cos(qa) = \cos(V_0) \cos(\kappa a) + \frac{E}{\kappa} \sin(V_0) \sin(\kappa a), \quad (26)$$

where we have set

$$\kappa = \sqrt{E^2 - m_0^2}. \quad (27)$$

Equation (26) defines the dispersion relation of the relativistic Kronig–Penney model, which has been investigated by several authors (see, for instance, [124, 126, 129]). The ordinary non-relativistic limit of the Kronig–Penney model is attained from (26) and (27) for $V_0 \ll 1$ and for energies E close to m_0 , for which the energy-momentum relation (27) reduces to the non-relativistic one ($E \simeq m_0 + \kappa^2/(2m_0)$); in this regime, the dispersion relation (26) reduces to $\cos(qa) = \cos(\kappa a) + (m_0 V_0 / \kappa) \sin(\kappa a)$, which is the ordinary dispersion relation encountered in the non-relativistic Kronig–Penney model. For larger energies E

but still for a low barrier area $V_0 \ll 1$, non-relativistic effects come into play as perturbative effects, which modify positions and widths of the allowed energy bands. Non-relativistic effects deeply modify the band structure of the crystal for potential strengths V_0 of the order ~ 1 . In particular, if V_0 is an integer multiple of π , all band gaps disappear and the dispersion relation reduces to the one of a relativistic free particle ((16) with $V(z) = 0$), as if the δ barriers were absent. In a FBG, the Dirac–Kronig–Penney model simply corresponds to an infinitely extended uniform FBG with a superimposed periodic sequence of lumped phase slips of equal amplitude $\Delta\phi = 2V_0$ and spaced by the distance a . The circumstance that the effects of the δ barriers disappear in the Dirac–Kronig–Penney model when V_0 is an integer multiple of π is simply due to the fact that, under such a condition, the phase slips are integer multiples of 2π , and thus the grating has no phase defects and mimics the dynamics of a one-dimensional free relativistic Dirac particle. A special case of the Dirac–Kronig–Penney model corresponds to the case $V_0 = \pi/2$. In this case, the resulting superstructure FBG comprises a periodic sequence of π phase slips, which has been proposed and demonstrated to realize slowing down of optical pulses [142, 143]. The band structure of the Dirac–Kronig–Penney model is simply mapped into the alternation of stop/transmission bands observed in spectrally resolved transmission measurements of the FBG. An example of the spectral transmission features of a superstructure FBG with periodic π phase slips, in which the allowed spectral transmission bands reproduce the band structure of the Dirac–Kronig–Penney model, is shown in Fig. 7.

If the periodic potential $V(z)$ is truncated, surface Tamm states do appear. Such states for the relativistic Kronig–Penney model attracted some interest in earlier papers by several authors [125, 129, 136–141], and a lively debate was raised about the proper boundary conditions that should be imposed to the relativistic wave function at a δ barrier. As earlier works [125, 136–138] suggested that the relativistic treatment yields a new class of surface states (the so-called Dirac surface states) which do not correspond to the common Tamm states in the non-relativistic limit, it was subsequently realized that application of more physical boundary conditions does not yield any surface state which violates the Tamm condition in the non-relativistic limit [139]. The relativistic extension of the Tamm model is defined by the potential (see, for instance, [129, 139])

$$V(z) = \begin{cases} V_1, & z < 0, \\ V_0 \sum_{n=1}^{\infty} \delta(z - na), & z > 0. \end{cases} \quad (28)$$

Surface states are found as localized solutions to (16), near the surface $z = 0$, satisfying the appropriate boundary conditions, as discussed in [139]. In our photonic system, the potential $V(z)$ defined by (28) and supporting the surface

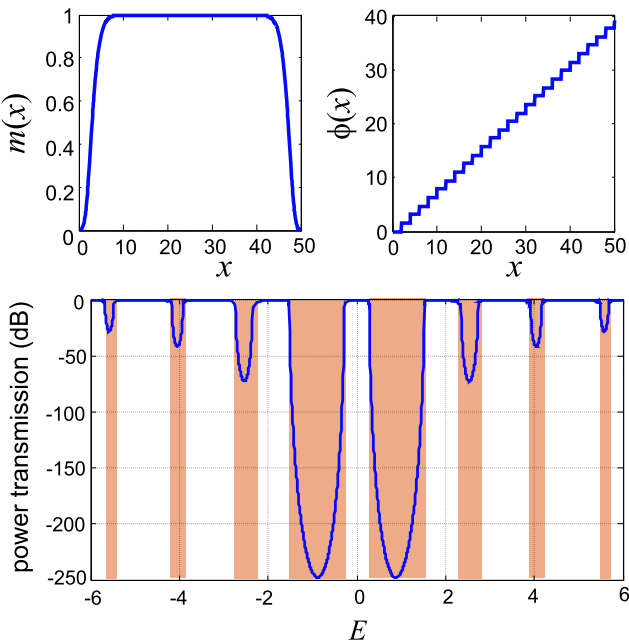


Fig. 7 Photonic realization of the Dirac–Kronig–Penney model in a superstructure FBG comprising a periodic sequence of π phase slips. The figure shows the spectral power transmission of the grating with amplitude and phase profiles given in the upper insets. Parameter values are $V_0 = \pi/2$, $a = 2$, $m_0 = 1$, and $L = 50$. The dashed areas are the stop bands of the corresponding Dirac–Kronig–Penney infinite lattice

Tamm states at the $z = 0$ boundary is basically realized by two adjacent sections of uniform grating regions but with different grating periods, with the second grating region (at $z > 0$) comprising a sequence of equally spaced phase slips, at a distance a , equal to $\Delta\phi = 2V_0$. The existence of surface states can be simply recognized by the appearance of narrow resonance peaks embedded in a stop-band region of the transmission spectrum of the grating (for more details we refer the reader to [96]).

7 Photonic realizations of non-Hermitian relativistic wave equations

Since the seminal paper by Bender and Boettcher [144], great attention has been devoted toward the investigation of non-Hermitian extensions of quantum mechanics and quantum field theories. Indeed, many works have remarked that the Hermiticity of the underlying Hamiltonian can be relaxed, and that a consistent quantum theory can be constructed for a broader class of Hamiltonians [145–148], in particular those possessing parity-time (\mathcal{PT}) symmetry. Non-Hermitian Hamiltonians are also very often found in reduced descriptions of open Hermitian quantum systems, with important applications to atomic, molecular, and condensed-matter physics [149–151]. Several recent

works have shown that optical structures in media with a complex refractive index can provide an experimentally accessible test bed to simulate in a purely classical setting non-Hermitian features rooted in the non-relativistic Schrödinger equation with a complex potential [152–161]. Recently, non-Hermitian extensions of relativistic wave equations [162–171] and non-Hermitian quantum field theories [172–175] have attracted an increasing interest as well; however, their physical realizations remain mostly unexplored. In Ref. [103], optical simulations of non-Hermitian wave equations have been proposed, which are based on light propagation in distributed-feedback (DFB) optical structures with controlled gain and/or loss regions.

Let us indicate by $n(z) = n_0 - \Delta n h(z) \cos(2\pi z/\Lambda + 2\theta(z))$ the effective index grating of the DFB structure, where n_0 is the modal refractive index in the absence of the grating, $\Delta n \ll n_0$ and Λ are the peak index change and the nominal period of the grating, respectively, and $h(z)$ and $2\theta(z)$ are the normalized amplitude and phase profiles, respectively, of the grating. For a pure index grating, $h(z)$ is real valued, whereas for a pure gain grating $h(z)$ is purely imaginary; in the most general case $h(z)$ can be taken to be complex valued [176]. The periodic modulation of the refractive index leads to Bragg scattering between two counterpropagating waves at frequencies close to the Bragg frequency $\omega_B = \pi c/(\Lambda n_0)$. The linear space-dependent absorption coefficient of counterpropagating waves in the structure is indicated by $\alpha_0(z)$ ($\alpha_0 > 0$ in lossy regions, $\alpha_0 < 0$ in gain regions). In a semiconductor DFB structure, gain and loss regions could be tailored by a judicious control of current injection across the active layer [176]. Indicating by $E(z, \tau) = \psi_1(z, \tau) \exp[-i\omega_B \tau + ik_B z + i\theta(z)] + \psi_2(z, \tau) \exp[-i\omega_B \tau - ik_B z - i\theta(z)] + c.c.$ the electric field propagating in the DFB structure, where $k_B = \pi/\Lambda$, the envelopes ψ_1 and ψ_2 of counterpropagating waves satisfy coupled-mode equations [176]. After introduction of the scaled space and time variables $x = z/Z$ and $t = \tau/T$, with $Z = 2n_0\Lambda/(\pi\Delta n)$ and $T = Z/v_g$, where $v_g \simeq c/n_0$ is the group velocity of light at frequency ω_B , the envelopes ψ_1 and ψ_2 satisfy the following Dirac-type equation in the Weyl representation [103]:

$$i\partial_t \psi = -i\sigma_z \partial_x \psi + \sigma_x m(x) \psi + V(x) \psi \equiv H \psi \quad (29)$$

with complex-valued mass m and vector potential V given by

$$m(x) = h(x), \quad V(x) = \frac{d\theta}{dx} - i\gamma(x), \quad (30)$$

where $\gamma(x) = Z\alpha_0(x)$ is the dimensionless absorption coefficient and $\sigma_{x,z}$ are the Pauli matrices. In a DFB structure, both $m(x)$ and $V(x)$ have a limited support over a spatial length L (the grating region), i.e. $m = V = 0$ for $|x| > L/2$.

Since H is non-Hermitian, its spectrum is generally complex valued; however, it could happen that, in spite of non-Hermiticity, the energy spectrum remains real valued, like in \mathcal{PT} symmetric Hamiltonians in the unbroken symmetry phase. In addition, because of the non-self-adjointness of H , spectral singularities could arise in the spectrum of H , which correspond to either a zero-width resonance in the transmission/reflection spectrum of the DFB (the threshold for self oscillation) [103, 157] or to a perfect absorption of radiation under a suitable two-port coherent excitation of the DFB structure [103, 177, 178]. Examples of non-Hermitian Dirac Hamiltonians showing such two different kinds of spectral singularities were discussed in Ref. [103] assuming a pure index grating (i.e. $h(x)$ real valued) for either \mathcal{PT} -invariant or \mathcal{PT} -non-invariant DFB structures. Another interesting example of a non-Hermitian relativistic wave equation is obtained by considering a purely gain grating (h purely imaginary) in the absence of absorption losses and chirp ($V = 0$). In this case, for an infinitely long grating ($L \rightarrow \infty$, $m = im_0$ constant, with m_0 real valued) (29) represents a superluminal extension of the relativistic Dirac equation [179–181] describing a freely moving hypothetical tachyonic particle, corresponding to a negative mass square at rest (see e.g. [182, 183]). A remarkable property of such an equation, in addition to enabling a kind of superluminal propagation, is the possibility to make a DFB structure fully transparent, as recently discussed in Ref. [184]. Tachyonic extensions of Dirac equations can be realized as well in two-dimensional honeycomb photonic lattices made of coupled waveguides with alternating gain and loss regions (a complex photonic graphene), as recently proposed in Ref. [104].

8 Conclusion and outlook

In this article, a brief overview of the possibility offered by light transport in periodic photonic structures to simulate in a purely classical setting the optical analogues of a wide variety of quantum phenomena rooted in relativistic wave equations has been presented. Spatial or temporal light transport in engineered photonic lattices and Bragg grating structures can simulate the Zitterbewegung of a relativistic electron, Klein tunneling, vacuum decay and pair production, the Dirac oscillator, the relativistic Kronig–Penney model, and certain non-Hermitian extensions of the Dirac equations, including superluminal (tachyonic) wave equations. Further quantum-optical analogies are expected to be investigated and to be implemented in experiments using waveguide lattices and passive/active Bragg grating and DFB structures.

Acknowledgements The author acknowledges financial support by the Italian MIUR (Grant No. PRIN-2008-YCAAK, project ‘Analogie ottico-quantistiche in strutture fotoniche a guida d’onda’).

References

1. D. Dragoman, M. Dragoman, *Quantum–Classical Analogies* (Springer, Berlin, 2004)
2. S. Longhi, *Laser Photonics Rev.* **3**, 243 (2009)
3. D.N. Christodoulides, F. Lederer, Y. Silberberg, *Nature* **424**, 817 (2003)
4. F. Lederer, G.I. Stegeman, D.N. Christodoulides, M. Segev, G. Assanto, Y. Silberberg, *Phys. Rep.* **463**, 1 (2008)
5. A. Szameit, S. Nolte, *J. Phys. B* **43**, 163001 (2010)
6. S. Longhi, in *Dynamical Tunneling: Theory and Experiment*, ed. by S. Keshavamurthy, P. Schlagheck (CRC Press/Taylor & Francis, Boca Raton, 2011), pp. 311–338
7. U. Peschel, T. Pertsch, F. Lederer, *Opt. Lett.* **23**, 1701 (1998)
8. R. Morandotti, U. Peschel, J.S. Aitchison, H.S. Eisenberg, Y. Silberberg, *Phys. Rev. Lett.* **83**, 4756 (1999)
9. T. Pertsch, P. Dannberg, W. Elflein, A. Bräuer, F. Lederer, *Phys. Rev. Lett.* **83**, 4752 (1999)
10. G. Lenz, I. Talanina, C.M. de Sterke, *Phys. Rev. Lett.* **83**, 963 (1999)
11. N. Chiodo, G. Della Valle, R. Osellame, S. Longhi, G. Cerullo, R. Ramponi, P. Laporta, U. Morgner, *Opt. Lett.* **31**, 1651 (2006)
12. H. Trompeter, W. Krolikowski, D.N. Neshev, A.S. Desyatnikov, A.A. Sukhorukov, Yu.S. Kivshar, T. Pertsch, U. Peschel, F. Lederer, *Phys. Rev. Lett.* **96**, 053903 (2006)
13. R. Khomeriki, S. Ruffo, *Phys. Rev. Lett.* **94**, 113904 (2005)
14. H. Trompeter, T. Pertsch, F. Lederer, D. Michaelis, U. Streppe, A. Bräuer, U. Peschel, *Phys. Rev. Lett.* **96**, 023901 (2006)
15. A. Fratalocchi, G. Assanto, K.A. Brzakiewicz, M.A. Karpierz, *Opt. Lett.* **31**, 1489 (2006)
16. A. Fratalocchi, G. Assanto, *Opt. Express* **14**, 2021 (2006)
17. S. Longhi, *Europhys. Lett.* **76**, 416 (2006)
18. F. Dreisow, A. Szameit, M. Heinrich, T. Pertsch, S. Nolte, A. Tünnermann, S. Longhi, *Phys. Rev. Lett.* **102**, 076802 (2009)
19. S. Longhi, *Opt. Lett.* **30**, 2137 (2005)
20. S. Longhi, M. Marangoni, M. Lobino, R. Ramponi, P. Laporta, E. Cianci, V. Foglietti, *Phys. Rev. Lett.* **96**, 243901 (2006)
21. R. Iyer, J.S. Aitchison, J. Wan, M.M. Dignam, C.M. de Sterke, *Opt. Express* **15**, 3212 (2007)
22. F. Dreisow, M. Heinrich, A. Szameit, S. Döring, S. Nolte, A. Tünnermann, S. Fahr, F. Lederer, *Opt. Express* **16**, 3474 (2008)
23. A. Szameit, I.L. Garanovich, M. Heinrich, A.A. Sukhorukov, F. Dreisow, T. Pertsch, S. Nolte, A. Tünnermann, Y.S. Kivshar, *Nat. Phys.* **5**, 271 (2009)
24. A. Joushaghani, R. Iyer, J.K.S. Poon, J.S. Aitchison, C.M. de Sterke, J. Wan, M.M. Dignam, *Phys. Rev. Lett.* **103**, 143903 (2009)
25. S. Longhi, *Phys. Rev. B* **80**, 235102 (2009)
26. G. Della Valle, S. Longhi, *Opt. Lett.* **35**, 673 (2010)
27. A. Szameit, I.L. Garanovich, M. Heinrich, A.A. Sukhorukov, F. Dreisow, T. Pertsch, S. Nolte, A. Tünnermann, S. Longhi, Y.S. Kivshar, *Phys. Rev. Lett.* **104**, 223903 (2010)
28. I. Vorobeichik, E. Narevicius, G. Rosenblum, M. Orenstein, N. Moiseyev, *Phys. Rev. Lett.* **90**, 176806 (2003)
29. G. Della Valle, M. Ornigotti, E. Cianci, V. Foglietti, P. Laporta, S. Longhi, *Phys. Rev. Lett.* **98**, 263601 (2007)
30. A. Szameit, Y.V. Kartashov, F. Dreisow, M. Heinrich, T. Pertsch, S. Nolte, A. Tünnermann, V.A. Vysloukh, F. Lederer, L. Torner, *Phys. Rev. Lett.* **102**, 153901 (2009)
31. S. Longhi, D. Janner, M. Marano, P. Laporta, *Phys. Rev. E* **67**, 036601 (2003)
32. S. Longhi, M. Marangoni, D. Janner, R. Ramponi, P. Laporta, E. Cianci, V. Foglietti, *Phys. Rev. Lett.* **94**, 073002 (2005)
33. T. Schwartz, G. Bartal, S. Fishman, M. Segev, *Nature* **446**, 55 (2007)

34. Y. Lahini, A. Avidan, F. Pozzi, M. Sorel, R. Morandotti, D.N. Christodoulides, Y. Silberberg, Phys. Rev. Lett. **100**, 013906 (2008)
35. S. Longhi, Phys. Rev. Lett. **97**, 110402 (2006)
36. P. Biagioni, G. Della Valle, M. Ornigotti, M. Finazzi, L. Duó, P. Laporta, S. Longhi, Opt. Express **16**, 3762 (2008)
37. F. Dreisow, A. Szameit, M. Heinrich, T. Pertsch, S. Nolte, A. Tünnermann, S. Longhi, Phys. Rev. Lett. **101**, 143602 (2008)
38. Y.V. Kartashov, V.A. Vysloukh, L. Torner, Phys. Rev. Lett. **99**, 233903 (2007)
39. K. Shandarova, C.E. Ruter, D. Kip, K.G. Makris, D.N. Christodoulides, O. Peleg, M. Segev, Phys. Rev. Lett. **102**, 123905 (2009)
40. E. Paspalakis, Opt. Commun. **258**, 31 (2006)
41. S. Longhi, G. Della Valle, M. Ornigotti, P. Laporta, Phys. Rev. B **76**, 201101(R) (2007)
42. Y. Lahini, F. Pozzi, M. Sorel, R. Morandotti, D.N. Christodoulides, Y. Silberberg, Phys. Rev. Lett. **101**, 193901 (2008)
43. F. Dreisow, A. Szameit, M. Heinrich, R. Keil, S. Nolte, A. Tünnermann, S. Longhi, Opt. Lett. **34**, 2405 (2009)
44. F. Dreisow, M. Ornigotti, A. Szameit, M. Heinrich, R. Keil, S. Nolte, A. Tünnermann, S. Longhi, Appl. Phys. Lett. **95**, 261102 (2009)
45. S.G. Krivoshlykov, I.N. Sissakian, Opt. Quantum Electron. **11**, 393 (1979)
46. S. Longhi, Opt. Lett. **34**, 2736 (2009)
47. A. Szameit, F. Dreisow, M. Heinrich, R. Keil, S. Nolte, A. Tünnermann, S. Longhi, Phys. Rev. Lett. **104**, 150403 (2010)
48. G. Della Valle, S. Longhi, J. Phys. B **43**, 051002 (2010)
49. S. Longhi, Opt. Lett. **36**, 819 (2011)
50. S. Longhi, J. Phys. B **44**, 051001 (2011)
51. S. Longhi, Phys. Rev. A **83**, 034102 (2011)
52. S. Longhi, Phys. Rev. A **83**, 043835 (2011)
53. K.S. Novoselov, A.K. Geim, S.V. Morozov, D. Jiang, M.I. Katsnelson, I.V. Grigorieva, S.V. Dubonos, A.A. Firsov, Nature (London) **438**, 197 (2005)
54. S.Y. Zhou, G.-H. Gweon, J. Graf, A.V. Fedorov, C.D. Spataru, R.D. Diehl, Y. Kopelevich, D.-H. Lee, S.G. Louie, A. Lanzara, Nat. Phys. **2**, 595 (2006)
55. M.I. Katsnelson, K.S. Novoselov, A.K. Geim, Nat. Phys. **2**, 620 (2006)
56. C.W.J. Beenakker, Rev. Mod. Phys. **80**, 1337 (2008)
57. A.H. Castro Neto, F. Guinea, N.M. Peres, K.S. Novoselov, A.K. Geim, Rev. Mod. Phys. **81**, 109 (2009)
58. P.M. Alsing, J.P. Dowling, G.J. Milburn, Phys. Rev. Lett. **94**, 220401 (2005)
59. J. Schliemann, D. Loss, R.M. Westervelt, Phys. Rev. Lett. **94**, 206801 (2005)
60. A. Bermudez, M.A. Martin-Delgado, E. Solano, Phys. Rev. A **76**, 041801(R) (2007)
61. L. Lamata, J. Leon, T. Schatz, E. Solano, Phys. Rev. Lett. **98**, 253005 (2007)
62. G. Juzeliunas, J. Ruseckas, M. Lindberg, L. Santos, P. Ohberg, Phys. Rev. A **77**, 011802(R) (2008)
63. M. Johanning, A.F. Varón, C. Wunderlich, J. Phys. B **42**, 154009 (2009)
64. N. Goldman, A. Kubasiak, A. Bermudez, P. Gaspard, M. Lewenstein, M.A. Martin-Delgado, Phys. Rev. Lett. **103**, 035301 (2009)
65. S.L. Zhu, B.G. Wang, L.M. Duan, Phys. Rev. Lett. **98**, 260402 (2007)
66. T.M. Rusin, W. Zawadzki, Phys. Rev. D **82**, 125031 (2010)
67. K.L. Wang, T. Liu, M. Feng, K. Wang, Phys. Rev. A **82**, 064501 (2010)
68. Q. Zhang, J.B. Gong, C.H. Oh, Phys. Rev. A **81**, 023608 (2010)
69. D. Braun, Phys. Rev. A **82**, 013617 (2010)
70. J. Casanova, J.J. Garcia-Ripoll, R. Gerritsma, C.F. Roos, E. Solano, Phys. Rev. A **82**, 020101 (2010)
71. J.I. Cirac, P. Maraner, J.K. Pachos, Phys. Rev. Lett. **105**, 190403 (2010)
72. K. Huang, Am. J. Phys. **20**, 479 (1952)
73. O. Klein, Z. Phys. **53**, 157 (1929)
74. A.F. Young, P. Kim, Nat. Phys. **5**, 222 (2009)
75. N. Stander, B. Huard, D. Goldhaber-Gordon, Phys. Rev. Lett. **102**, 026807 (2009)
76. G.A. Steele, G. Gotz, L.P. Kouwenhoven, Nat. Nanotechnol. **4**, 363 (2009)
77. R. Gerritsma, B.P. Lanyon, G. Kirchmair, F. Zähringer, C. Hempel, J. Casanova, J.J. García-Ripoll, E. Solano, R. Blatt, C.F. Roos, Phys. Rev. Lett. **106**, 060503 (2011)
78. R. Gerritsma, G. Kirchmair, F. Zähringer, E. Solano, R. Blatt, C.F. Roos, Nature (London) **463**, 68 (2010)
79. F.D.M. Haldane, S. Raghu, Phys. Rev. Lett. **100**, 013904 (2008)
80. R.A. Sepkhanov, Ya.B. Bazaliy, C.W.J. Beenakker, Phys. Rev. A **75**, 063813 (2007)
81. O. Peleg, G. Bartal, B. Freedman, O. Manela, M. Segev, D.N. Christodoulides, Phys. Rev. Lett. **98**, 103901 (2007)
82. O. Bahat-Treidel, O. Peleg, M. Segev, Opt. Lett. **33**, 2251 (2008)
83. T. Ochiai, M. Onoda, Phys. Rev. B **80**, 155103 (2009)
84. X. Zhang, Phys. Rev. Lett. **100**, 113903 (2008)
85. O. Bahat-Treidel, O. Peleg, M. Grobman, N. Shapira, T. Pereg-Barnea, M. Segev, Phys. Rev. Lett. **104**, 063901 (2010)
86. O. Bahat-Treidel, O. Peleg, M. Segev, H. Buljan, Phys. Rev. A **82**, 013830 (2010)
87. D.Ö. Güney, D.A. Meyer, Phys. Rev. A **79**, 063834 (2009)
88. L.-G. Wang, Z.-G. Wang, J.-X. Zhang, S.-Y. Zhu, Opt. Lett. **34**, 1510 (2009)
89. L.-G. Wang, Z.-G. Wang, S.-Y. Zhu, Europhys. Lett. **86**, 47008 (2009)
90. S. Longhi, Opt. Lett. **35**, 235 (2010)
91. S. Longhi, Phys. Rev. B **81**, 075102 (2010)
92. S. Longhi, Phys. Rev. A **81**, 022118 (2010)
93. F. Dreisow, M. Heinrich, R. Keil, A. Tünnermann, S. Nolte, S. Longhi, A. Szameit, Phys. Rev. Lett. **105**, 143902 (2010)
94. S. Longhi, Phys. Res. Int. **2010**, 645106 (2010)
95. S. Longhi, Opt. Lett. **35**, 1302 (2010)
96. S. Longhi, Cent. Eur. J. Phys. **9**, 110 (2011)
97. S. Longhi, J. Phys. B **43**, 205402 (2010)
98. S.H. Nam, J. Zhou, A.J. Taylor, A. Efimov, Opt. Express **18**, 25329 (2010)
99. M.I. Molina, Y.S. Kivshar, Opt. Lett. **35**, 2895 (2010)
100. S. Bittner, B. Dietz, M. Miski-Oglu, P. Oriá Iriarte, A. Richter, F. Schäfer, Phys. Rev. B **82**, 014301 (2010)
101. M. Shen, L.X. Ruan, X. Chen, Opt. Express **18**, 12779 (2010)
102. S.H. Nam, A.J. Taylor, A. Efimov, Opt. Express **18**, 10120 (2010)
103. S. Longhi, Phys. Rev. Lett. **105**, 013903 (2010)
104. A. Szameit, M.C. Rechtsman, O. Bahat-Treidel, M. Segev, arXiv:1103.3389 (2011)
105. E. Schrödinger, Sitz. Preuss. Akad. Wiss. Phys.-Math. Kl. **24**, 418 (1930)
106. W. Greiner, *Relativistic Quantum Mechanics* (Springer, Berlin, 1990)
107. F. Cannata, L. Ferrari, G. Russo, Solid State Commun. **74**, 309 (1990)
108. A. Calogeracos, N. Dombey, Contemp. Phys. **40**, 313 (1999)
109. F. Sauter, Z. Phys. **69**, 742 (1931)
110. P. Christillin, E. d'Emilio, Phys. Rev. A **76**, 042104 (2007)
111. E.S. Fradkin, D.M. Gitman, Sh.M. Shvartsman, *Quantum Electrodynamics with Unstable Vacuum* (Springer, Berlin, 1991)
112. H.K. Avetissian, *Relativistic Nonlinear Electrodynamics* (Springer, New York, 2006)

113. J. Schwinger, Phys. Rev. **82**, 664 (1951)
114. E. Brezin, C. Itzykson, Phys. Rev. D **2**, 1191 (1970)
115. M. Ruf, G.R. Mocken, C. Müller, K.Z. Hatsagortsyan, C.H. Keitel, Phys. Rev. Lett. **102**, 080402 (2009)
116. M. Moshinsky, A. Szczepaniak, J. Phys. A **22**, L817 (1989)
117. M. Moshinsky, Y.F. Smirnov, *The Harmonic Oscillator in Modern Physics* (Harwood, Amsterdam, 1996)
118. R.P. Martínez-y-Romero, H.N. Nunez-Yepez, A.L. Salas-Brito, Eur. J. Phys. **16**, 135 (1995)
119. D. Ito, K. Mori, E. Carrieri, Nuovo Cimento **51A**, 1119 (1967)
120. J. Bentez, R.P. Martínez-y-Romero, H.N. Nuez-Yepez, A.L. Salas-Brito, Phys. Rev. Lett. **64**, 1643 (1990). *Erratum*, Phys. Rev. Lett. **65**, 2085 (1990)
121. R.P. Martínez-y-Romero, M. Moreno, A. Zentella, Phys. Rev. D **43**, 2036 (1991)
122. F. Dominguez-Adame, M.A. Gonzalez, Europhys. Lett. **13**, 193 (1990)
123. R.L. de Kronig, W.G. Penney, Proc. R. Soc. Lond. Ser. A **130**, 499 (1931)
124. F. Dominguez-Adame, Am. J. Phys. **55**, 1003 (1987)
125. S.G. Davison, M. Steslicka, J. Phys. C **2**, 1802 (1969)
126. B.H.J. McKellar, G.J. Stephenson, Phys. Rev. A **36**, 2566 (1987)
127. F. Dominguez-Adame, J. Phys., Condens. Matter **1**, 109 (1989)
128. I.M. Mladenov, Phys. Lett. A **131**, 313 (1989)
129. G.J. Clerck, B.H.J. McKellar, Phys. Rev. C **41**, 1198 (1990)
130. C.L. Roy, C. Basu, J. Phys. Chem. Solids **52**, 745 (1991)
131. F. Dominguez-Adame, A. Sanchez, Phys. Lett. A **159**, 153 (1991)
132. G.J. Clerck, B.H.J. McKellar, Phys. Rev. B **47**, 6942 (1993)
133. C. Basu, C.L. Roy, E. Macia, F. Dominguez-Adame, A. Sanchez, J. Phys. A **27**, 3285 (1994)
134. F. Dominguez-Adame, E. Macia, A. Khan, C.L. Roy, Physica B **212**, 67 (1995)
135. M. Barbier, F.M. Peeters, P. Vasilopoulos, J.M. Pereira, Phys. Rev. B **77**, 115446 (2008)
136. M.L. Glasser, S.G. Davison, Int. J. Quant. Chem. **4**, 867 (1970)
137. S.G. Davison, J.D. Levine, Solid State Phys. **25**, 32 (1970)
138. M. Steslicka, S.G. Davison, Phys. Rev. B **1**, 1858 (1970)
139. R. Subramanian, K.V. Bhagwat, J. Phys. C **5**, 798 (1972)
140. S. Yuyi, Surf. Sci. **108**, L477 (1981)
141. C.L. Roy, J.S. Pandey, Physica **137A**, 389 (1986)
142. D. Janner, G. Galzerano, G. Della Valle, P. Laporta, S. Longhi, M. Belmonte, Phys. Rev. E **72**, 056605 (2005)
143. S. Longhi, D. Janner, G. Galzerano, G. Della Valle, D. Gatti, P. Laporta, Electron. Lett. **41**, 1075 (2005)
144. C.M. Bender, S. Boettcher, Phys. Rev. Lett. **80**, 5243 (1998)
145. C.M. Bender, D.C. Brody, H.F. Jones, Phys. Rev. Lett. **89**, 270401 (2002)
146. A. Mostafazadeh, J. Math. Phys. **43**, 2814 (2002)
147. C.M. Bender, Rep. Prog. Phys. **70**, 947 (2007)
148. A. Mostafazadeh, Int. J. Geom. Methods Mod. Phys. **7**, 1191 (2010)
149. N. Moiseyev, Phys. Rep. **302**, 211 (1998)
150. J.G. Muga, J.P. Palao, B. Navarro, I.L. Egusquiza, Phys. Rep. **395**, 357 (1998)
151. I. Rotter, J. Phys. A **42**, 1 (2009)
152. A. Ruschhaupt, F. Delgado, J.G. Muga, J. Phys. A **38**, L171 (2005)
153. R. El-Ganainy, K.G. Makris, D.N. Christodoulides, Z.H. Musslimani, Opt. Lett. **32**, 2632 (2007)
154. K.G. Makris, R. El-Ganainy, D.N. Christodoulides, Z.H. Musslimani, Phys. Rev. Lett. **100**, 103904 (2008)
155. A. Guo, G.J. Salamo, D. Duchesne, R. Morandotti, M. Volatier-Ravat, V. Aimez, G.A. Siviloglou, D.N. Christodoulides, Phys. Rev. Lett. **103**, 093902 (2009)
156. S. Klaiman, U. Günther, N. Moiseyev, Phys. Rev. Lett. **101**, 080402 (2008)
157. A. Mostafazadeh, Phys. Rev. Lett. **102**, 220402 (2009)
158. S. Longhi, Phys. Rev. Lett. **103**, 123601 (2009)
159. S. Longhi, Phys. Rev. B **80**, 235102 (2009)
160. S. Longhi, Phys. Rev. A **81**, 022102 (2010)
161. C.E. Rüter, K.G. Makris, R. El-Ganainy, D.N. Christodoulides, M. Segev, D. Kip, Nat. Phys. **6**, 192 (2010)
162. C. Mudry, B.D. Simons, A. Altland, Phys. Rev. Lett. **80**, 4257 (1998)
163. H. Egrifes, R. Sever, Phys. Lett. A **344**, 117 (2005)
164. A. Sinha, P. Roy, Mod. Phys. Lett. A **20**, 2377 (2005)
165. C.S. Jia, A. de Souza Dutra, J. Phys. A **39**, 11877 (2006)
166. F. Cannata, A. Ventura, Phys. Lett. A **372**, 941 (2008)
167. O. Mustafa, S.H. Mazharimousavi, Int. J. Theor. Phys. **47**, 1112 (2008)
168. C.-S. Jia, A. de Souza Dutra, Ann. Phys. **323**, 566 (2008)
169. C.-S. Jia, P.-Q. Wang, J.-Y. Liu, S. He, Int. J. Theor. Phys. **47**, 2513 (2008)
170. V.G.C.S. dos Santos, A. de Souza Dutra, M.B. Hott, Phys. Lett. A **373**, 3401 (2009)
171. F. Cannata, A. Ventura, J. Phys. A **43**, 075305 (2010)
172. C.M. Bender, K.A. Milton, V.M. Savage, Phys. Rev. D **62**, 085001 (2000)
173. C.M. Bender, D.C. Brody, H.F. Jones, Phys. Rev. Lett. **93**, 251601 (2004)
174. C.M. Bender, S.F. Brandt, J.-H. Chen, Q. Wang, Phys. Rev. D **71**, 065010 (2005)
175. A. Mostafazadeh, Int. J. Mod. Phys. A **21**, 2553 (2006)
176. J. Carroll, J. Whiteaway, D. Plumb, *Distributed Feedback Semiconductor Lasers* (The Institution of Electrical Engineers, London, 1998)
177. S. Longhi, Phys. Rev. A **82**, 031801(R) (2010)
178. Y.D. Chong, L. Ge, A.D. Stone, Phys. Rev. Lett. **106**, 093902 (2011)
179. A. Chodosa, A.I. Hausera, Phys. Lett. B **150**, 431 (1985)
180. J. Ciborowski, J. Rembielinski, Eur. Phys. J. C **8**, 157 (1999)
181. T. Chang, G. Ni, Fizika B **11**, 49 (2002)
182. G. Feinberg, Phys. Rev. Lett. **159**, 1089 (1967)
183. O.M.P. Bilaniuk, E.C.G. Sudarshan, Phys. Today **22**, 43 (1969)
184. S. Longhi, Opt. Lett. **35**, 3844 (2010)